Title page

Improvement of biodistribution profile of a radiogallium-labeled, αvβ6 integrin-targeting peptide probe by incorporation of negatively charged amino acids

Short title: Effects of D6 linker

Shunsuke Nakamura, Aya Matsuno, Masashi Ueda

Department of Biofunction Imaging Analysis, Graduate School of Medicine, Dentistry, and Pharmaceutical Sciences, Okayama University, 1-1-1 Tsushima-naka, Kita-ku, Okayama 700-8530, Japan

Corresponding author

Masashi Ueda, Ph.D.

Department of Biofunction Imaging Analysis, Graduate School of Medicine, Dentistry, and Pharmaceutical Sciences, Okayama University, 1-1-1 Tsushima-naka, Kita-ku, Okayama 700-8530, Japan

E-mail: mueda@cc.okayama-u.ac.jp

The type of article: Original article

Abstract

Objective: Pancreatic ductal adenocarcinoma (PDAC) is one of the most lethal cancers. Since αvβ6 integrin has been reported as a promising target for PDAC diagnosis, we previously developed H-Cys(mal-NOTA-^{67}Ga)-(Gly)6-A20FMDV2-NH_2 ([^{67}Ga]CG6) as an αvβ6 integrin-targeting probe. Although [^{67}Ga]CG6 specifically binds to αvβ6 integrin-positive xenografts, the uptake of [^{67}Ga]CG6 in the organs surrounding the pancreas, such as the liver and spleen, was comparable to that in the αvβ6 integrin-positive xenografts. We hypothesized that the undesirable accumulation of [^{67}Ga]CG6 in those organs was caused by the positive charges of [^{67}Ga]CG6 (+3). In this study, we aimed to decrease [^{67}Ga]CG6 uptake in the liver and spleen by reducing the electric charges of the probe.

Methods: We synthesized H-Cys(mal-NOTA-^{67}Ga)-(Asp)6-A20FMDV2-NH_2 ([^{67}Ga]CD6) and evaluated its affinity to αvβ6 integrin via in vitro competitive binding assay. Isoelectric points of the probes were determined by electrophoresis. Biodistribution study, autoradiography, and immunostaining for β6 integrin were conducted using αvβ6 integrin-positive and negative tumor-bearing mice.

Results: In vitro competitive binding assay showed that the alteration of the linker had a negligible impact on the affinity of [^{67}Ga]CG6 to αvβ6 integrin. The results of

electrophoresis revealed that [^{67}Ga]CG6 was positively charged whereas [^{67}Ga]CD6 was negatively charged. In the biodistribution study, the uptake of [^{67}Ga]CD6 in the αvβ6 integrin-positive xenografts was significantly higher than that in the αvβ6 integrin-negative ones at 60 and 120 minutes. The uptake of [^{67}Ga]CD6 in the liver and spleen was more than 2-fold lower than that of [^{67}Ga]CG6 at both time points. In the immunohistochemistry study, the radioactivity accumulated areas in the autoradiogram of the αvβ6 integrin-positive xenograft coincided with β6 integrin-expressing areas.

Conclusion: We have successfully reduced the nonspecific uptake in the liver and spleen by altering the linker amino acid from G6 to D6. [^{67}Ga]CD6 overcame the drawbacks of [^{67}Ga]CG6 in its biodistribution.

Keywords:

αvβ6 integrin; Pancreatic ductal adenocarcinoma (PDAC); A20FMDV2; Aspartic acids; Electric charge

Introduction

Pancreatic ductal adenocarcinoma (PDAC) is one of the most malignant cancers in humans, and is a major cause of cancer-related deaths [1]. Despite recent medical developments, it is difficult to develop new effective therapies, and hence PDAC is expected to become the second leading cause of cancer deaths by 2030 [2]. Under current circumstances, the most effective treatment for PDAC is surgical resection, and therefore it is thought that early detection of PDAC closely correlates with a patient's prognosis. However, the initial symptoms of PDAC lack specific clinical features, therefore, it is challenging to detect PDAC at an operable stage [3].

An epithelial-specific cell surface receptor, αvβ6 integrin, is usually undetectable in healthy adult tissues. The expression of αvβ6 integrin, however, is significantly upregulated in many malignant cancers, and αvβ6 integrin is involved in the migration, invasion, and proliferation of tumor cells [4-9]. Previously, it was reported that almost all PDAC patients had positive αvβ6 integrin expression, and the significant upregulation of αvβ6 integrin in PDAC was closely related to the malignancy of PDAC [5, 10]. Willemieke *et al*. previously reported that αvβ6 integrin was an excellent biomarker to differentiate PDAC from other tissues and to identify tumor-positive lymph nodes [11]. Due to this data, we focused on αvβ6 integrin as a

promising target for both the prognosis and detection of PDAC.

A20FMDV2 (NAVPNLRGDLQVLAQKVART) is a 20-amino acid peptide derived from an envelope protein of the foot-and-mouth disease virus [12]. A20FMDV2 shows a high affinity and selectivity to αvβ6 integrin [13], therefore this peptide has been used for positron emission tomography (PET) and single-photon emission computed tomography (SPECT) imaging studies such as [^{18}F]FBA-PEG28-A20FMDV2-PEG28 [14], ^{64}Cu-labeled A20FMDV2 [15], [^{123}I]IFMDV2 [3], and [^{111}In]DTPA-A20FMDV2 [16]. In our previous study, we focused on gallium-68 ($T_{1/2}$ = 68 minutes) because it is a generator-produced radionuclide and does not require a cyclotron on site, unlike fluorine-18 and copper-64. In order to develop a ^{68}Ga-labeled A20FMDV2 peptide, we synthesized H-Cys(mal-NOTA-^{nat}Ga)-(Gly)n-A20FMDV2-NH_2 (n = 1, 4, 6, 8), and discovered that the G6 linker (n = 6) was the most appropriate length not to hamper the binding of the peptide to αvβ6 integrin between the N-terminus of A20FMDV2 and the cysteine residue which was conjugated with maleimide-NOTA. The H-Cys(mal-NOTA-^{67}Ga)-(Gly)6-A20FMDV2-NH_2 (termed [^{67}Ga]CG6) showed high affinity and specificity to αvβ6 integrin in vivo [17]. However, [^{67}Ga]CG6 tended to accumulate in the organs surrounding the pancreas, such as the liver and spleen, at the

same level as αvβ6 integrin-positive xenografts, hence, it seemed that [^{67}Ga]CG6 was not suitable for the diagnosis of the primary PDAC.

We hypothesized that the undesirable accumulation of [^{67}Ga]CG6 in those organs was caused by the positive charges of [^{67}Ga]CG6, since the theoretical charge of the probe was +3. In this study, we designed and synthesized H-Cys(mal-NOTA-^{67}Ga)-(Asp)6-A20FMDV2-NH_2 (termed [^{67}Ga]CD6) containing the D6 linker, instead of the G6 linker, to reduce the positive charge of [^{67}Ga]CG6. We aimed to evaluate the utility of [^{67}Ga]CD6 as an αvβ6 integrin imaging agent and compare the biodistribution of [^{67}Ga]CG6 with that of [^{67}Ga]CD6.

Materials and Methods

General

The 9-fluorenylmethyloxycarbonyl (Fmoc)-protected amino acids, Fmoc-NH-SAL-MBHA Resin, and coupling agents (*O*-(1*H*-benzotriazol-1-yl)-*N*,*N*,*N'*,*N'*-tetramethyluronium hexafluorophosphate, 1-hydroxy-1*H*-benzotriazole hydrate, and *N*,*N*-diisopropylethylamine) were purchased from Watanabe Chemical Industries, Ltd. (Hiroshima, Japan).

2,2′-(7-(2-((2-(2,5-dioxo-2,5-dihydro-1*H*-pyrrol-1-yl)ethyl)amino)-2-oxoethyl)-1,4,7-tri azonane-1,4-diyl)diacetic acid (maleimide-NOTA) was purchased from CheMatech (Dijon, France). Gallium-67 chloride was kindly supplied and gallium-67 citrate was purchased from FUJIFILM Toyama Chemical Co., Ltd. (Tokyo, Japan). Immobiline DryStrip pH3-11 (7 cm) and the IPG buffer pH3-11 were purchased from GE Healthcare (Boston, USA). Reversed-phase high-performance liquid chromatography (RP-HPLC) was performed on a Cosmosil 5C_{18}-AR-II column (4.6 × 150 mm for analytical RP-HPLC and 10 × 250 mm for preparative RP-HPLC; Nacalai Tesque, Inc., Kyoto, Japan) using a 28% v/v acetonitrile in 0.1% v/v trifluoroacetic acid/H_2O as a mobile phase at a flow rate of 1.0 mL/min for analytical RP-HPLC and 4.0 mL/min for preparative RP-HPLC. The eluate was monitored via the detection of its proper absorption at 220-230 nm.

Animal experiments were performed in accordance with the guidelines of the Okayama University Animal Care Committee. The experimental procedures performed were approved by the committee.

Peptide synthesis and maleimide-NOTA conjugation

Peptides were synthesized by Fmoc solid-phase peptide synthesis using an

automated peptide synthesizer (PSSM-8; Shimadzu Corporation, Kyoto, Japan) according to a previously described method [18]. These peptides were extended using Fmoc-NH-SAL-MBHA Resin as a starting material. The crude peptides were purified by preparative RP-HPLC before lyophilization.

Maleimide-NOTA was incubated with purified peptides in a 0.2 M ammonium acetate buffer (pH 6.5, 100 μL) at room temperature for 60 minutes. The crude NOTA-peptides were also purified by preparative RP-HPLC before lyophilization.

To obtain nonradioactive authentic probes, the purified NOTA-peptides were incubated with $Ga(NO_3)_3$ in 100 μL of water at 80ºC for 15 minutes. The crude Ga-NOTA-peptides were purified via preparative RP-HPLC before lyophilization.

The identities below were determined by analytical RP-HPLC and electrospray ionization mass spectroscopy (API4000; SCIEX, Framingham, MA).

[^{nat}Ga]CG6: calculated for $C_{126}H_{212}GaN_{44}O_{41}S$ $[M+3H]^{3+}$; *m/z*, 1034.5; found, 1035.2.

[^{nat}Ga]CD6: calculated for $C_{138}H_{224}GaN_{44}O_{53}S$ $[M+3H]^{3+}$; *m/z*, 1150.5; found, 1151.0.

Cells and Cell culture

AsPC-1 and MIA PaCa-2 human pancreatic carcinoma cells were obtained

from the European Collection of Authenticated Cell Cultures and the RIKEN BRC Cell Engineering Division, respectively. Both cells were cultured as previously described [17].

Competitive binding assay

The affinity of [^{nat}Ga]CD6 to αvβ6 integrin was evaluated by competitive binding assay using [^{125}I]IFMDV2 as a radioligand (n = 4). The Ki value of [^{nat}Ga]CD6 was calculated by using GraphPad Prism 7 (GraphPad Software, Inc., San Diego, CA). Preparation of [^{125}I]IFMDV2 and binding assay were conducted according to a previously described method [3].

Isoelectric point evaluation

The purified peptides (100-200 μg) were dissolved in 125 μL sample buffer (8 M urea, 20% v/v glycerol, 0.5% IPG buffer) and an Immobiline Dry strip was saturated with the solution. Electrophoresis was performed in four steps (1. Hold [300 V, 30 minutes], 2. Gradient [1,000 V, 30 minutes], 3. Gradient [5,000 V, 80 minutes], 4. Hold [5,000V, 25 minutes]) on Ettan IPGphor 3 (GE Healthcare). Immobilization of the peptides in the gels was performed with 12.5% v/v glutaraldehyde/H_2O for 60 minutes,

and the gels were washed 3 times with washing buffer (30% v/v methanol and 10% v/v acetic acid in water). Thereafter, the gels were stained by Coomassie brilliant blue (CBB) solution (0.02% w/v CBB and 0.10% w/v copper sulfate in washing buffer) for 60 minutes, and were then washed 3 times with washing buffer. The bands derived from the peptides in the gels were detected by Chemidoc XRS (Bio-Rad Laboratories, Inc., Hercules, USA). The pI values were determined according to the manufacturer's protocol.

The pI values of both peptides containing non-amidated C-terminus were calculated by the ProtParam tool (http://web.expasy.org/protparam/).

Radiolabeling

The purified NOTA-peptides (20-40 μg) were incubated with $^{67}GaCl_3$ or ^{67}Ga-citrate (2-15 MBq) in 0.2 M sodium acetate buffer (100-300 μL, pH 4.0) at 80ºC for 15 minutes. The reaction solution was then purified by analytical RP-HPLC.

Log P determination

[^{67}Ga]CG6 or [^{67}Ga]CD6 was added into an equal volume (500 μL:500 μL) mixture of *n*-octanol and 25 mM phosphate buffer (pH7.4). After vigorous shaking for

30 minutes, the mixture was centrifuged at 5,000 rpm for 5 minutes. Samples from both *n*-octanol and aqueous layers were obtained, and their radioactivity was measured. The partition coefficients (log *P*-values) were calculated as the average of three independent measurements.

In vitro plasma stability evaluation

Preparation of the rodent plasma and stability evaluation of [^{67}Ga]CD6 were performed according to a previously described method [17].

Animal model

Male severe combined immunodeficiency mice (C.B-17/Icr-scid Jcl) at 4 weeks of age were purchased from CLEA Japan, Inc. (Tokyo, Japan). Models of AsPC-1 and MIA PaCa-2 xenografts were prepared according to a previously described method [3].

Biodistribution

[^{67}Ga]CG6 or [^{67}Ga]CD6 (100 kBq/100 μL) were injected intravenously into tumor bearing mice (n = 3-8) in the tail vein. The mice were killed at 10, 60, and 120

minutes after probe administration. Whole organs were immediately harvested and weighed, and their radioactivity was measured. The results were expressed as the percentage injected dose per gram (%ID/g).

Autoradiography and Immunostaining

[^{67}Ga]CD6 (1.5 MBq/100 μL) was injected intravenously into tumor bearing mice (n = 4) in the tail vein, and the mice were killed 60 minutes after probe administration. The tumors were removed and frozen in hexane (-80ºC), and the frozen tumors were sliced into 10 μm-thick sections with a cryomicrotome (CM1860; Leica Microsystems, Wetzlar, Germany). The sections were exposed to an imaging plate for 20 hours, and autoradiograms were obtained with a Typhoon FLA 7000 (GE Healthcare). The adjacent sections used for autoradiography were incubated with 1:100 diluted anti-β6 integrin mAb (Millipore, Burlington, USA) at 4ºC for 12 hours as a primary antibody. After incubation, these sections were incubated with 1:200 diluted anti-mouse IgG, horseradish peroxidase-linked whole antibody (GE Healthcare) at 4ºC for 12 hours. Finally, DAB and hematoxylin staining were performed. Photo data were acquired using an Olympus BX53 microscope (Olympus Corporation, Tokyo, Japan).

Statistical analysis

The data are expressed as mean ± standard deviation. The Mann Whitney *U*-test was performed by using GraphPad Prism 7 to evaluate statistical significance. A *P* value < 0.05 was considered statistically significant.

Results

Binding affinity to αvβ6 integrin

The calculated Ki value of [^{67}Ga]CD6 was 4.4 ± 2.0 nM, and was comparable to that of [^{67}Ga]CG6 (3.5 ± 0.3 nM [17]). This finding indicated that the linker alteration from G6 to D6 had a negligible impact on the binding affinity to αvβ6 integrin.

Isoelectric point evaluation

Pictures of CBB stained gels are shown in Fig. 1. The band of CG6-A20FMDV2 was detected at the anode side, and that of CD6-A20FMDV2 was detected at the cathode side. The calculated and measured pI values are shown in Table 1. It was confirmed that CG6-A20FMDV2 was positively charged and CD6-A20FMDV2 was negatively charged. There were slight differences between the

measured pI values and the calculated ones. We used C-terminal amidated peptides for pI determination, however the ProtParam tool cannot calculate pI values of peptides containing modified amino acids. Therefore, the measured pI values are more basic than the calculated values.

Radiolabeling

Analytical HPLC chromatograms of [$^{nat/67}$Ga]CG6 and [$^{nat/67}$Ga]CD6 are shown in Fig. 2. The radiochemical yield of [^{67}Ga]CG6 and [^{67}Ga]CD6 was 55-69%. The radiochemical purity of both probes was > 95%.

Log P determination

The Log *P*-values of [^{67}Ga]CG6 and [^{67}Ga]CD6 were -2.96 ± 0.14 and -2.88 ± 0.26, respectively.

In vitro stability evaluation

The extraction rate of radioactivity from the plasma was 53.0 ± 3.0%. The recovery of radioactivity from the HPLC column was 87.2 ± 0.7%. The percentages of intact [^{67}Ga]CD6 at 60 and 120 minutes were 86.7 ± 1.0% and 71.4 ± 5.7%,

respectively.

Biodistribution

Biodistribution of each probe was evaluated in mice bearing AsPC-1 (αvβ6 integrin positive) and MIA PaCa-2 (αvβ6 integrin negative) xenografts. The results are shown in Table 2. Biodistribution data of [^{67}Ga]CG6 was consistent with our previous report [17]. The highest accumulation of both probes was observed in the kidneys, and moderate accumulation was observed in αvβ6 integrin-positive organs, such as the stomach and intestine. The uptake of [^{67}Ga]CD6 in the AsPC-1 xenografts was significantly higher than that in the MIA PaCa-2 xenografts after 60 minutes, and the uptake of [^{67}Ga]CD6 in the AsPC-1 xenografts was similar to that of [^{67}Ga]CG6. Focusing on the uptake of both probes in the organs surrounding the pancreas, the uptake of [^{67}Ga]CG6 in the liver and spleen was comparable to that in the AsPC-1 xenografts. Conversely, the uptake of [^{67}Ga]CD6 in the liver and spleen was significantly lower than that in the AsPC-1 xenografts after 60 minutes ($P < 0.05$, Mann-Whitney *U*-test). Compared to [^{67}Ga]CG6, the uptake of [^{67}Ga]CD6 in the liver and spleen was reduced by 73% ($P = 0.057$) and 83% ($P < 0.05$), respectively at 120 minutes.

Autoradiography and histological analysis

To confirm the in vivo specificity of [^{67}Ga]CD6 toward αvβ6 integrin, we compared the areas of accumulated radioactivity with the β6 integrin-expressing areas in the tumors. Figure 3 shows the autoradiograms and β6 integrin immunostaining of each tumor section. With immunostaining, β6 integrin was strongly expressed in the AsPC-1 xenograft, while it was hardly detected in the MIA PaCa-2 xenograft. The areas of accumulated radioactivity in the autoradiogram of the AsPC-1 xenograft roughly coincided with the αvβ6 integrin-expressing areas. However, the areas where [^{67}Ga]CD6 accumulated in an independent manner of αvβ6 integrin expression were also observed in AsPC-1 and MIA PaCa-2 xenografts.

Discussion

In the present study, we designed and synthesized [^{67}Ga]CD6 to reduce the undesirable accumulation which would be derived from the positive charge of [^{67}Ga]CG6. In vitro competitive binding assay revealed that the alteration of the linker between the N-terminus of A20FMDV2 and the cysteine residue had a negligible

impact on the binding affinity to αvβ6 integrin. In the biodistribution study, the uptake of [^{67}Ga]CD6 in the AsPC-1 xenografts was significantly higher than that in the MIA PaCa-2 xenografts at 60 and 120 minutes. The uptake of [^{67}Ga]CD6 in the organs surrounding the pancreas was more than 2-fold lower than that of [^{67}Ga]CG6 at both time points. This data suggested that [^{67}Ga]CD6 overcame the drawbacks of [^{67}Ga]CG6 in its biodistribution.

The uptake of [^{67}Ga]CD6 in almost all normal organs was at a similar level with that of [^{67}Ga]CG6, except for in the liver and spleen. The uptake of [^{67}Ga]CD6 in the liver and spleen was approximately 3.5-fold and 6-fold less than that of [^{67}Ga]CG6, respectively, at 120 minutes. The cell membrane is generally negatively charged. Yamamoto *et al*. demonstrated that negatively charged micelles avoided non-specific accumulation in the liver and spleen, compared with neutral ones, which was attributable to the electrostatic repulsion [19]. Conversely, it was reported that highly negatively charged nanoparticles are easier to be opsonized than neutral and positively charged ones, and are easily taken up by macrophages in the reticuloendothelial system (RES) such as the liver and spleen [20]. However, Xiao *et al*. reported that nanoparticles with slightly negative charge showed the lowest uptake in the liver, and they estimated that it was attributed to not only the electrostatic repulsion but also the low opsonization

rate [20]. Interestingly, a slightly negative charge has favorable effects on not only nanoparticles but also peptides. Other researchers reported that the introduction of the slightly negative charge to ^{99m}Tc-labeled bombesin analogues was one of the best way to reduce the liver uptake and improve their pharmacokinetic profile [21]. These results suggested that slightly negatively charged carriers could minimize the recognition and non-specific accumulation by macrophages in the RES. In this study, isoelectric point evaluation indicated that [^{67}Ga]CD6 was more negatively charged than [^{67}Ga]CG6. Therefore, the reduction of the [^{67}Ga]CD6 uptake in the liver and spleen can be explained by the difference of the electric charge between [^{67}Ga]CG6 and [^{67}Ga]CD6. [^{67}Ga]CD6 is the first radiolabeled A20FMDV2 derivative that charged negatively. Our findings may be contributing to the design of negatively-charged, novel A20FMDV2 derivative probes. However, it is difficult to determine a preferable range of the electric charge of A20FMDV2-derived probes from our result. Garcia *et al*. evaluated the biodistribution of peptide probes that have various charges (+1, 0, -1, and -2). The radioactivity in the liver decreased in an amount-dependent manner of the negative charges [21]. The theoretical electric charge of [^{67}Ga]CD6 was -3. From the viewpoint of liver accumulation, this value would meet a criterion because the liver accumulation of [^{67}Ga]CD6 was more than 2-fold lower than that of [^{67}Ga]CG6, with an electric

charge of +3. Recently, we also succeeded in reduction of undesirable accumulation in the liver and spleen by N-acetylation of [^{67}Ga]CG6 [17]. The theoretical net charge of acetylated [^{67}Ga]CG6 (Ac-[^{67}Ga]CG6) is +2. The accumulation of Ac-[^{67}Ga]CG6 in the liver (0.26 ± 0.03 %ID/g at 120 minutes) and spleen (0.14 ± 0.01 %ID/g at 120 minutes) was at a similar level with that of [^{67}Ga]CD6 in the liver and spleen at the same time point. As per tumoral accumulation, Ac-[^{67}Ga]CG6 showed approximately 1.3-fold higher accumulation (2.02 ± 0.22 %ID/g at 120 minutes) than [^{67}Ga]CD6 did. This finding is in accordance with the previously reported result by Garcia *et al*. that the most negatively charged probe did not show the best tumoral accumulation [21]. Therefore, it may be possible that the electric charge of -3 is too low to maintain the tumoral accumulation of [^{67}Ga]CD6. To determine a preferable range of the electric charge, it is necessary to evaluate the biodistribution of A20FMDV2-derived probes with a charge from +1 to -2.

In the ARG study, there were some areas where [^{67}Ga]CD6 accumulated independent of αvβ6 integrin expression. The accumulation of [^{67}Ga]CD6 in such areas would be derived from the non-specific binding. The results of in vivo blocking studies performed previously indicated that the accumulation of A20FMDV2-derived probes in αvβ6-integrin-positive xenografts was not completely blocked. The percentage of

radioactivity decrease was approximately 40-60% in the blocking group [3, 16, 17]. Therefore, [^{67}Ga]CD6 may also have characteristics showing moderate non-specific binding.

Previously, it was reported that Ga-complex conjugated oligo-aspartic acids, [$^{67/68}$Ga]DOTA-(Asp)n, strongly bound to hydroxyapatite, a major component of the bone [22]. [^{68}Ga]DOTA-D11-c(RGDfK) was also reported to be a potential PET probe for the diagnosis of primary cancer lesions, in addition to simultaneously diagnosing osteoblastic and osteolytic bone metastases [23]. Similar to these probes, [^{67}Ga]CD6 might allow for the visualization of primary cancer lesions and bone metastases. However, the bone uptake of [^{67}Ga]CD6 was low (less than 1 %ID/g) at all time points examined, hence the D6 linker in [^{67}Ga]CD6 was not of sufficient length to interact with hydroxyapatite in the bone.

A major problem of low molecular weight probes labeled by metallic radionuclides is the high and persistent radioactivity level in the kidneys [24]. Specifically, cationic probes will strongly interact with the brush border membrane on the proximal tubules because the membrane is negatively charged [21, 25]. In the previous study regarding [^{111}In]DTPA-octreotide derivatives, the uptake of [^{111}In]DTPA-Asp-D-Phe-octreotide in the kidneys was remarkably lower than that of

[^{111}In]DTPA-D-Phe-octreotide due to its negative charge [25]. In the current study, the uptake of [^{67}Ga]CD6 in the kidneys was lower than that of [^{67}Ga]CG6 at 60 and 120 minutes after administration. Similar to [^{111}In]DTPA-Asp-D-Phe-octreotide, this reduction of the renal radioactivity can be explained by the negative charge of [^{67}Ga]CD6. However, renal radioactivity remained high and persistent. Therefore, the modification of the electric charges of [^{67}Ga]CD6 alone was insufficient to reduce renal radioactivity. These results suggested that further improvements of [^{67}Ga]CD6 to reduce the radioactivity in the kidneys are needed, such as the introduction of metabolizable linkers, such as NOTA-Met-Ile-maleimide or NOTA-Met-Val-Lys-maleimide [24, 26].

Several PET probes based on the A20FMDV2 peptide have already been reported. Hausner *et al*. developed [^{18}F]FBA-A20FMDV2 [12, 27] and [^{18}F]FBA-PEG28-A20FMDV2-PEG28 [14], and both probes were potent αvβ6 integrin imaging agents, in vivo. Particularly, [^{18}F]FBA-A20FMDV2 was evaluated in healthy human subjects and was confirmed safe [28]. The uptake of [^{67}Ga]CD6 in the αvβ6 integrin-positive xenografts (1.86 ± 0.34 %ID/g at 60 minutes) was superior to [^{18}F]FBA-A20FMDV2 (0.69 ± 0.19 %ID/g at 60 minutes), but inferior to [^{18}F]FBA-PEG28-A20FMDV2-PEG28 (4.7 ± 0.9 %ID/g at 60 minutes) [14, 27], although direct comparison was difficult because the biodistribution studies were

conducted using different cell lines. Hausner *et al*. also reported that the bi-terminal PEGylation of A20FMDV2 improved not only its tumor retention but also its tumor uptake [14, 27]. In the current study, the N- and C-termini of [^{67}Ga]CD6 were not modified by polyethylene glycol (PEG). Therefore, the bi-terminal PEGylation of [^{67}Ga]CD6 should have favorable influences on its targeting capability.

[^{67}Ga]CD6 highly accumulated in the stomach and intestine which were organs surrounding the pancreas. It is reported that αvβ6 integrin physiologically expresses strongly in mouse stomach and moderately in mouse intestine [16]. However, the first-in-human study of [^{18}F]FBA-A20FMDV2 revealed that the radioactivity accumulation in the stomach and intestine was at a similar level as the liver and cleared lineally in a log-scale graph [28]. Therefore, PDAC might be detected by [$^{67/68}$Ga]CD6 in clinical settings.

Conclusion

[^{67}Ga]CD6 showed high binding affinity to αvβ6 integrin not only in vitro but also in vivo. Replacement of the linker amino acid from Gly to Asp provided a negative charge to the probe, resulting in the reduction of non-specific accumulation in the liver

and spleen. The replacement of the linker amino acid did not affect tumoral accumulation of the probe. Therefore, [^{67}Ga]CD6 overcame the drawbacks of [^{67}Ga]CG6 in its biodistribution.

References

[1] Siegel RL, Miller KD, and Jemal A. Cancer Statistics, 2017. CA Cancer J Clin 2017;67:7-30.

[2] Rahib L, Smith BD, Aizenberg R, Rosenzweig AB, Fleshman JM, and Matrisian LM. Projecting cancer incidence and deaths to 2030: the unexpected burden of thyroid, liver, and pancreas cancers in the United States. Cancer Res 2014;74:2913-21.

[3] Ueda M, Fukushima T, Ogawa K, Kimura H, Ono M, Yamaguchi T, et al. Synthesis and evaluation of a radioiodinated peptide probe targeting αvβ6 integrin for the detection of pancreatic ductal adenocarcinoma. Biochem Biophys Res Commun 2014;445:661-6.

[4] Desai K, Nair MG, Prabhu JS, Vinod A, Korlimarla A, Rajarajan S, et al. High expression of integrin β6 in association with the Rho-Rac pathway identifies a poor prognostic subgroup within HER2 amplified breast cancers. Cancer Med

2016;5:2000-11.

[5] Niu J and Li Z. The roles of integrin αvβ6 in cancer. Cancer Lett 2017;403:128-37.

[6] Zhang ZY, Xu KS, Wang JS, Yang GY, Wang W, Wang JY, et al. Integrin αvβ6 acts as a prognostic indicator in gastric carcinoma. Clin Oncol (R Coll Radiol) 2008;20:61-6.

[7] Yang GY, Guo S, Dong CY, Wang XQ, Hu BY, Liu YF, et al. Integrin αvβ6 sustains and promotes tumor invasive growth in colon cancer progression. World J Gastroenterol 2015;21:7457-67.

[8] Thomas GJ, Nystrom ML, and Marshall JF. αvβ6 integrin in wound healing and cancer of the oral cavity. Journal of oral pathology & medicine : official publication of the International Association of Oral Pathologists and the American Academy of Oral Pathology 2006;35:1-10.

[9] Hezel AF, Deshpande V, Zimmerman SM, Contino G, Alagesan B, O'Dell MR, et al. TGF-β and αvβ6 integrin act in a common pathway to suppress pancreatic cancer progression. Cancer Res 2012;72:4840-5.

[10] Notni J, Reich D, Maltsev OV, Kapp TG, Steiger K, Hoffmann F, et al. In Vivo PET Imaging of the Cancer Integrin αvβ6 Using ^{68}Ga-Labeled Cyclic RGD Nonapeptides. J Nucl Med 2017;58:671-7.

[11] Tummers WS, Farina-Sarasqueta A, Boonstra MC, Prevoo HA, Sier CF, Mieog JS, et al. Selection of optimal molecular targets for tumor-specific imaging in pancreatic ductal adenocarcinoma. Oncotarget 2017;8:56816-28.

[12] Hausner SH, DiCara D, Marik J, Marshall JF, and Sutcliffe JL. Use of a peptide derived from foot-and-mouth disease virus for the noninvasive imaging of human cancer: generation and evaluation of 4-[^{18}F]fluorobenzoyl A20FMDV2 for in vivo imaging of integrin αvβ6 expression with positron emission tomography. Cancer Res 2007;67:7833-40.

[13] Kapp TG, Rechenmacher F, Neubauer S, Maltsev OV, Cavalcanti-Adam EA, Zarka R, et al. A Comprehensive Evaluation of the Activity and Selectivity Profile of Ligands for RGD-binding Integrins. Sci Rep 2017;7:39805.

[14] Hausner SH, Bauer N, Hu LY, Knight LM, and Sutcliffe JL. The Effect of Bi-Terminal PEGylation of an Integrin αvβ6-Targeted ^{18}F Peptide on Pharmacokinetics and Tumor Uptake. J Nucl Med 2015;56:784-90.

[15] Hu LY, Bauer N, Knight LM, Li Z, Liu S, Anderson CJ, et al. Characterization and evaluation of ^{64}Cu-labeled A20FMDV2 conjugates for imaging the integrin αvβ6. Mol Imaging Biol 2014;16:567-77.

[16] Saha A, Ellison D, Thomas GJ, Vallath S, Mather SJ, Hart IR, et al. High-resolution

in vivo imaging of breast cancer by targeting the pro-invasive integrin αvβ6. J Pathol 2010;222:52-63.

[17] Ui T, Ueda M, Higaki Y, Kamino S, Sano K, Kimura H, et al. Development and characterization of a ^{68}Ga-labeled A20FMDV2 peptide probe for the PET imaging of αvβ6 integrin-positive pancreatic ductal adenocarcinoma. Bioorg Med Chem 2020;28:115189.

[18] Ueda M, Ogawa K, Miyano A, Ono M, Kizaka-Kondoh S, and Saji H. Development of an oxygen-sensitive degradable peptide probe for the imaging of hypoxia-inducible factor-1-active regions in tumors. Mol Imaging Biol 2013;15:713-21.

[19] Yamamoto Y, Nagasaki Y, Kato Y, Sugiyama Y, and Kataoka K. Long-circulating poly(ethylene glycol)-poly(D,L-lactide) block copolymer micelles with modulated surface charge. J Control Release. 2001;77:27-38.

[20] Xiao K, Li Y, Luo J, Lee JS, Xiao W, Gonik AM, et al. The effect of surface charge on in vivo biodistribution of PEG-oligocholic acid based micellar nanoparticles. Biomaterials 2011;32:3435-46.

[21] Garcia Garayoa E, Schweinsberg C, Maes V, Brans L, Blauenstein P, Tourwe DA, et al. Influence of the molecular charge on the biodistribution of bombesin analogues labeled with the [^{99m}Tc(CO)$_3$]-core. Bioconjug Chem 2008;19:2409-16.

[22] Ogawa K, Ishizaki A, Takai K, Kitamura Y, Kiwada T, Shiba K, et al. Development of novel radiogallium-labeled bone imaging agents using oligo-aspartic acid peptides as carriers. PLoS One 2013;8:e84335.

[23] Ogawa K, Yu J, Ishizaki A, Yokokawa M, Kitamura M, Kitamura Y, et al. Radiogallium Complex-Conjugated Bifunctional Peptides for Detecting Primary Cancer and Bone Metastases Simultaneously. Bioconjug Chem 2015;26:1561-70.

[24] Uehara T, Rokugawa T, Kinoshita M, Nemoto S, Fransisco Lazaro GG, Hanaoka H, et al. $^{67/68}$Ga-labeling agent that liberates $^{67/68}$Ga-NOTA-methionine by lysosomal proteolysis of parental low molecular weight polypeptides to reduce renal radioactivity levels. Bioconjug Chem 2014;25:2038-45.

[25] Oshima N, Akizawa H, Zhao S, Zhao Y, Nishijima K, Kitamura Y, et al. Design, synthesis and biological evaluation of negatively charged ^{111}In-DTPA-octreotide derivatives. Bioorg Med Chem 2014;22:1377-82.

[26] Uehara T, Yokoyama M, Suzuki H, Hanaoka H, and Arano Y. A Gallium-67/68-Labeled Antibody Fragment for Immuno-SPECT/PET Shows Low Renal Radioactivity Without Loss of Tumor Uptake. Clin Cancer Res 2018;24:3309-16.

[27] Hausner SH, Abbey CK, Bold RJ, Gagnon MK, Marik J, Marshall JF, et al. Targeted in vivo imaging of integrin αvβ6 with an improved radiotracer and its

relevance in a pancreatic tumor model. Cancer Res 2009;69:5843-50.

[28] Keat N, Kenny J, Chen K, Onega M, Garman N, Slack RJ, et al. A Microdose PET Study of the Safety, Immunogenicity, Biodistribution, and Radiation Dosimetry of ^{18}F-FB-A20FMDV2 for Imaging the Integrin αvβ6. J Nucl Med Technol 2018;46:136-43.

Acknowledgment

The authors are grateful to FUJIFILM Toyama Chemical Co., Ltd. for providing gallium-67 chloride. The authors gratefully thank Division of Instrumental Analysis, Department of Instrumental Analysis & Cryogenics, Advanced Science Research Center, Okayama University for the use of the peptide synthesizer; the Department of Genomics & Proteomics, Advanced Science Research Center, Okayama University for the use of the Ettan IPGphor 3; and the Department of Radiation Research, Shikata Laboratory, Advanced Science Research Center, Okayama University for assistance in our experiments using radioisotopes. This work was supported in part by a grant from the Pancreas Research Foundation of Japan and the Takeda Science Foundation. The authors declare that they have no conflict of interest.

Table 1. Calculated and measured pI values of peptides

Peptides	Calculated pI †	Measured pI
H-Cys-(Gly)6-A20FMDV2-NH_2 (CG6-A20FMDV2)	9.5	10-11
H-Cys-(Asp)6-A20FMDV2-NH_2 (CD6-A20FMDV2)	4.0	4-5

†: The pI values were calculated by the ProtParam tool (https://web.expasy.org/protparam/), regarding the peptide sequence as H-Cys-X6-A20FMDV2-OH (X = Gly or Asp).

Table 2. Biodistribution of [^{67}Ga]CG6 and [^{67}Ga]CD6 in tumor-bearing mice

	10 min		60 min		120 min	
Organ	[^{67}Ga]CG6	[^{67}Ga]CD6	[^{67}Ga]CG6	[^{67}Ga]CD6	[^{67}Ga]CG6	[^{67}Ga]CD6
Blood	1.52 ± 0.57	1.11 ± 0.25	0.54 ± 0.11	0.46 ± 0.19	0.41 ± 0.11	0.22 ± 0.02
AsPC-1	1.69 ± 0.32	2.01 ± 0.46	1.83 ± 0.40	1.86 ± 0.34†	1.18 ± 0.21	1.51 ± 0.24†
MIA PaCa-2	2.06 ± 0.23	1.72 ± 0.75	0.55 ± 0.12	0.49 ± 0.10	0.57 ±0.06	0.35 ± 0.05
Pancreas	2.96 ± 1.05	1.78 ± 0.42	0.87 ± 0.39	0.81 ± 0.12	0.86 ± 0.09	0.65 ± 0.05*
Liver	1.64 ± 0.77	0.55 ± 0.07	1.03 ± 0.38	0.31 ± 0.05**	1.10 ± 0.50	0.30 ± 0.10
Spleen	1.52 ± 0.88	0.49 ± 0.16	1.02 ± 0.48	0.49 ± 0.36	1.27 ± 0.60	0.21 ± 0.04*
Heart	2.68 ± 0.28	1.73 ± 0.30	1.82 ± 0.25	1.27 ± 0.48*	1.29 ± 0.04	1.09 ± 0.06
Lung	4.95 ± 1.25	3.32 ± 0.57	4.51 ± 0.79	1.84 ± 0.34**	3.26 ± 1.18	1.43 ± 0.21
Muscle	2.39 ± 0.67	1.23 ± 0.32	2.07 ± 0.33	1.44 ± 0.14*	1.70 ± 0.38	1.29 ± 0.40
Stomach	13.42 ± 3.62	19.01 ± 2.48	15.08 ± 2.88	17.85 ± 5.72	12.09 ± 2.16	13.48 ± 2.62
Intestine	7.37 ± 1.45	11.90 ± 1.63	6.02 ± 1.34	9.35 ± 1.37*	5.58 ± 1.02	7.30 ± 0.36
Kidney	85.84 ± 8.69	97.43 ± 3.99	128.02 ± 13.22	95.56 ± 13.31*	123.14 ± 16.18	109.13 ± 14.98
Bone	n.d.	0.89 ± 0.19	n.d.	0.54 ± 0.13	n.d.	0.52 ± 0.11

Organ uptake values expressed as percent injected dose per gram of tissue.

The bone uptake of [^{67}Ga]CG6 was not measured at all time points examined (n.d., not

determined).

Values are represented as mean ± S.D., n = 3-8.

* and ** indicate $P < 0.05$ and $P < 0.01$ versus the uptake of [^{67}Ga]CG6 at the same time points, respectively (Mann Whitney *U*-test).

† indicates $P < 0.05$ versus the uptake of [^{67}Ga]CD6 in the MIA PaCa-2 xenografts at the same points (Mann-Whitney *U*-test).

Figures

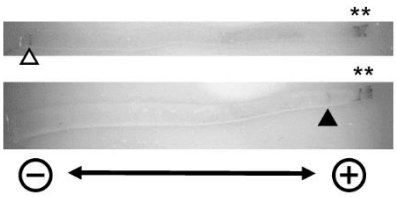

Fig. 1 The Coomassie brilliant blue (CBB) stained strip gels containing CG6-A20FMDV2 (upper) and CD6-A20FMDV2 (bottom).

The white and black arrowheads indicate the bands of CG6-A20FMDV2 and CD6-A20FMDV2, respectively. * indicates cracks caused by the electrodes, not the bands derived from the peptides.

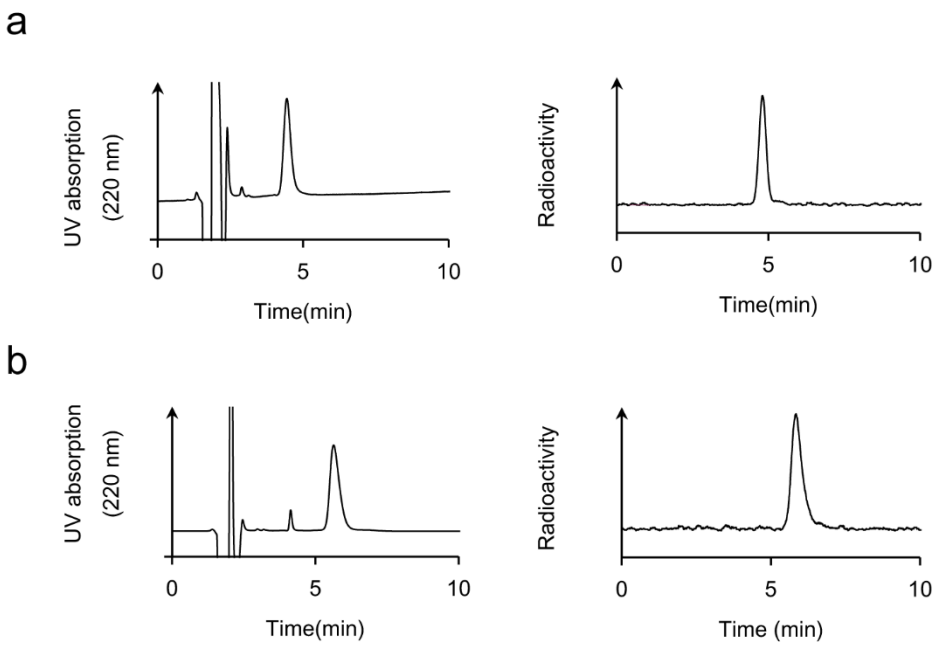

Fig. 2 Typical analytical HPLC chromatograms of [$^{nat/67}$Ga]CG6 and [$^{nat/67}$Ga]CD6. (a) HPLC chromatograms of [^{nat}Ga]CG6 (left) and [^{67}Ga]CG6 (right). The retention time of [^{nat}Ga]CG6 and [^{67}Ga]CG6 were 4.44 and 4.81 min, respectively. (b) HPLC chromatograms of [^{nat}Ga]CD6 (left) and [^{67}Ga]CD6 (right). The retention time of [^{nat}Ga]CD6 and [^{67}Ga]CD6 were 5.64 and 5.84 min, respectively.

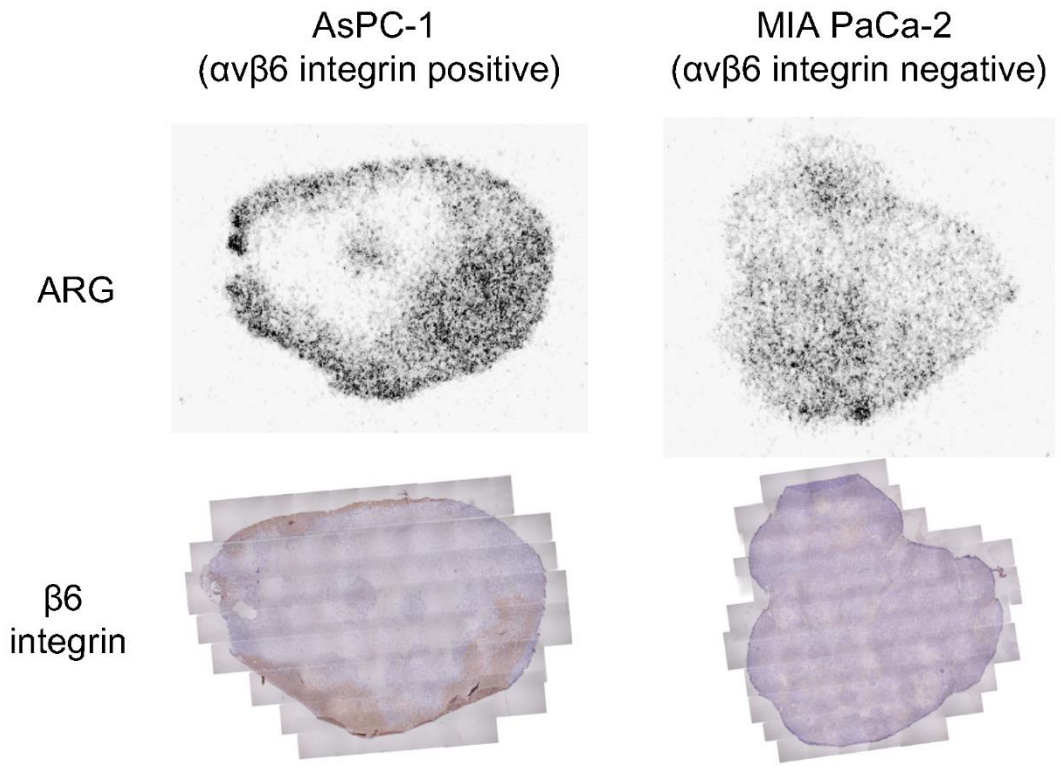

Fig. 3 Representative images of autoradiograms (ARG) and β6 integrin immunostaining in the AsPC-1 and MIA PaCa-2 tumor sections.

β6 integrin only dimerized with αv integrin, and thus the β6 integrin-expressing areas are regarded as the αvβ6 integrin-expressing area. The β6 integrin-positive areas (brown) were roughly coincided with the radioactivity accumulation areas in the AsPC-1 xenograft.